Selection of Λ^0 Production Events in MicroBooNE

MICROBOONE-NOTE-1097-PUB

The MicroBooNE Collaboration
microboone_info@fnal.gov

October 2021

Abstract

A selection to find Cabibbo suppressed Λ production events, $\bar{\nu}_\mu + \mathrm{Ar} \to \mu^+ + \Lambda^0 + X$, in the MicroBooNE detector is described. This channel is sensitive to cross section and final state interaction parameters in different ways and can help break their degeneracy. Λ^0 production events are distinguished from background by the existence of a secondary vertex created when the Λ^0 decays. The selection examines a list of reconstructed particles thought to be the result of a neutrino interaction, first finding a muon candidate, then a proton and π^- candidate and testing their consistency with a $\Lambda^0 \to p + \pi^-$ decay. The selection achieves an efficiency of approximately 7% while rejecting 99.9999% of the background. This selection is designed to study neutrino interactions in the NuMI flux. After applying the selection, Monte Carlo simulation predicts 9.0 ± 0.8 (MC stat.) signal and 3.1 ± 1.4 background events when combining 1.0×10^{21} protons on target of neutrino mode flux and 1.3×10^{21} protons on target of anti-neutrino mode flux, corresponding to a significance of 2.6 σ.

Contents

1 Introduction

This note presents a strategy for the identification of neutrino interactions resulting in the Cabibbo suppressed production of a Λ^0 baryon in the MicroBooNE Liquid Argon Time Projection Chamber (LArTPC). The ultimate goal of this analysis is to measure the cross section of the process:

$$\bar{\nu}_\mu + \mathrm{Ar} \rightarrow \mu^+ + \Lambda^0 + X \tag{1}$$

X denotes any additional final state particles with zero strangeness. This is distinct from associated hyperon production, when a K meson or anti-hyperon is produced in addition to the hyperon and there is no change in total strangeness. Most calculations of neutrino-nucleus cross sections factorise the process into two parts: an initial interaction between the neutrino and a nucleon/group of nucleons and final state interactions (FSI) between the resulting particles and the rest of the nucleus. The hadronic final state is sensitive to both stages and their effects can be difficult to disentangle with data. The different hyperon production channels are affected by neutrino-nucleon cross section physics and final state interaction effects in different ways and could help break their degeneracy [1]. This channel is exclusively driven by anti-neutrinos and could be used to characterise this part of the flux for future LArTPC experiments such as the Deep Underground Neutrino Experiment or the Short Baseline Neutrino Program. The lack of a neutrino channel, in combination with Cabibbo suppression and higher kinematic thresholds than charged current quasi-elastic interactions result in a very low event rate, necessitating a powerful selection to remove the very large quantity of background.

MicroBooNE receives flux from two neutrino beams, the Booster Neutrino Beam (BNB) and Neutrinos at the Main Injector (NuMI). The BNB has exclusively operated in neutrino mode over MicroBooNE's data taking period, while NuMI has run in a mix of neutrino mode (forward horn current, FHC) and anti-neutrino mode (reverse horn current, RHC). MicroBooNE is approximately 6° off axis from NuMI which results in a richer anti-neutrino flux in both modes compared with the BNB. For this reason we search for Λ^0 events in the NuMI flux.

1.1 Simulation

Beamline geometry, hadron and neutrino production are simulated using Geant 4 which is used to generate samples of neutrinos crossing a 30 m × 30 m window close to the detector geometry, which can then be read by a neutrino event generator. We study the predictions of two neutrino event generators, GENIE [2] and NuWro [3], which employ different direct hyperon production models. In particular, NuWro includes final state interactions for hyperons [1] while GENIE does not. Both generators simulate the interactions of neutrinos from the beam in the MicroBooNE geometry producing a set of final state particles. Their propagation and any subsequent secondary interactions or decays are modelled using Geant4 [4]. A detector simulation then models the response to this activity, such as charge collected by TPC wires and light flashes recorded by photomultiplier tubes.

In this analysis we use the Pandora multi-algorithm pattern recognition/reconstruction framework [5], which reconstructs the activity in the detector into three dimensional tracks and showers. If a potential neutrino interaction vertex is identified, Pandora will create a reconstructed primary vertex and collect the tracks and showers thought to be the result of the interaction (and their children and grandchildren etc. if they exist) into a hierarchy of reconstructed particles. The selection studies this collection of reconstructed objects.

Aside from real neutrino interactions in the cryostat, two other sources of activity must be included: neutrino interactions outside the cryostat resulting in particles crossing the active volume, labelled as “dirt" in this document, and cosmic rays crossing the detector (in the absence of a neutrino interaction), labelled as “EXT". Dirt interactions are always simulated with GENIE. In many of the figures of this document the in-cryostat component is further divided into signal events, other direct hyperon production events (such as Σ^0 generation) and all other neutrino interaction processes.

1.2 Selection Strategy

The decay of the Λ^0 is Cabbibo suppressed and it may live long enough to travel a few centimeters in MicroBooNE, with the primary decay mode being $\Lambda^0 \rightarrow p + \pi^-$ (BF = 64% [6]). This, in combination with the anti-muon, produces a very distinctive signature, two examples of which are shown in Figure 1. The selection tries to identify the two components of this signature, the activity left by the muon and the activity left by the decay.

We begin with a preselection, described in Section 2, that rejects events lacking the structure required by the remainder of the selection. Next, in Section 3, we identify reconstructed particles corresponding to the μ and $p+\pi^-$ produced by the decaying Λ^0. From these we obtain quantities such as the invariant mass of the decay products that can distinguish a real Λ^0 decay from other sources of protons and pions, described in Section 4. Finally some topological tests are performed with the chosen muon, proton and pion candidates to confirm the decay products form a true secondary vertex, which are explained in Section 5.

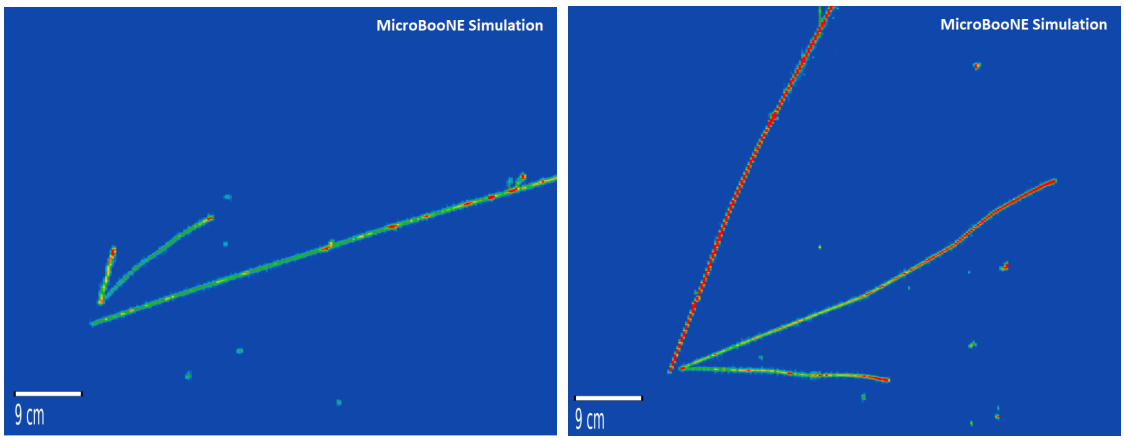

Figure 1: Examples of simulated $\bar{\nu}_\mu + \mathrm{Ar} \rightarrow \mu^+ + \Lambda^0 + X$ events. The V shaped green/red regions correspond to the proton and pion produced through the Λ's decay.

1.3 Signal Definition and Predicted Events

The signal in this analysis includes any anti-neutrino interactions that satisfy the following:

1. The interaction of a muon-anti-neutrino occurred resulting in the direct production of a Λ^0 or Σ baryon: $\bar{\nu}_\mu + N \rightarrow \mu^+ + \Lambda^0, \Sigma^0, \Sigma^-$. Other sources of hyperons such as $\Lambda^0 + K$ production or strangeness violating FSI are excluded.

2. The hyperon exiting the nucleus is a Λ^0. This can result from a Λ^0 produced in the anti-neutrino-nucleon interaction surviving to the final state or a Σ baryon converting to a Λ during FSI.

3. The Λ^0 subsequently decays via $\Lambda^0 \rightarrow p + \pi^-$.

4. The resulting proton and π^- have true momenta greater than 300 MeV/c and 100 MeV/c respectively.

5. The true interaction vertex in located in the fiducial volume (FV). In this analysis the fiducial volume described in [7] is used, which consists of a series of hexagonal prisms excluding small regions of the top and corners of the detector that suffer from the strongest space charge effects [8].

With this signal definition, the number of predicted signal events from each flux and event generator combination are presented in Table 1.

Event Generator	FHC Events	RHC Events
GENIE	54 ± 2	73 ± 2
NuWro	56 ± 2	64 ± 2

Table 1: Predicted number of signal events. Uncertainties are Monte Carlo statistical only.

2 Preselection

The Pandora reconstruction package will not always generate a candidate neutrino vertex if there is no suitable activity in the event, which aids with cosmic rejection. The first requirement applied by the preselection is that there must be a reconstructed neutrino vertex and that it must, after correction for space charge effects [8], be located in the same fiducial volume used to define the signal.

Pandora classifies reconstructed particles as either track-like or shower-like. Typically track-like particles correspond to muons, protons, and charged pions, while shower-like particles are primarily photons and electrons/positrons which induce electromagnetic showers. The three final state particles in the signal are all track-like and so the first selection requirement is that the set of reconstructed particles contains at least three tracks and no showers. The number of tracks and showers for the various event categories are presented in Figures 2 and 3. Combined, these three cuts remove approximately 99.9% of the background events.

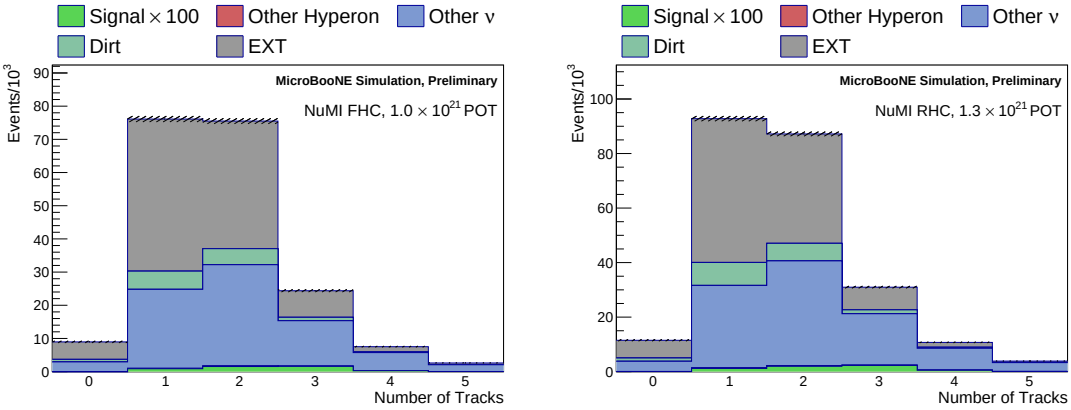

(a) GENIE, FHC

(b) GENIE, RHC

Figure 2: Predicted number of tracks in the Pandora reconstructed particle hierarchy for events passing the fiducial volume cut. All events with fewer than three tracks are rejected by the preselection. The hatched regions indicate the MC statistical uncertainty. The signal component has been scaled up by a factor of 100.

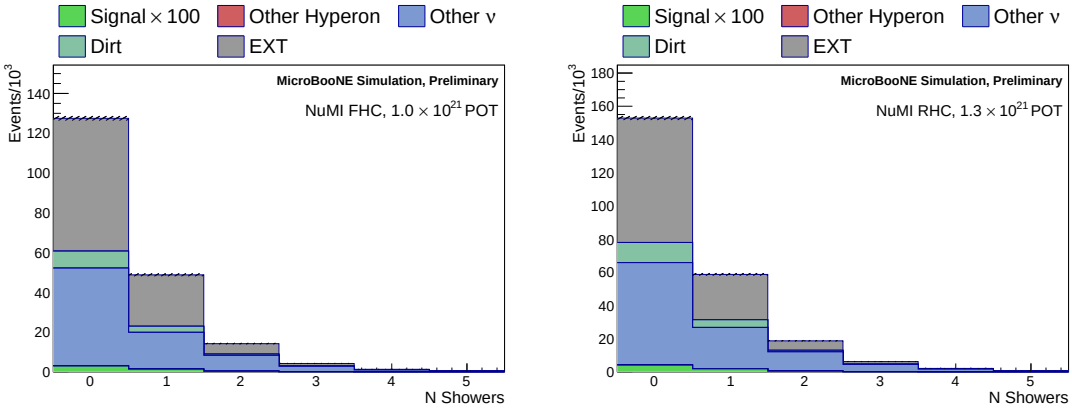

(a) GENIE, FHC

(b) GENIE, RHC

Figure 3: Predicted number of showers in the Pandora reconstructed particle hierarchy for events passing the fiducial volume cut. All events with fewer than three tracks are rejected by the preselection. The signal component has been scaled up by a factor of 100.

3 Muon, Decay Proton and Decay Pion Identification

Subsequent steps of the selection consist of calculating several quantities that distinguish a Λ^0 decay from other pairs of tracks produced at a common vertex, such as their invariant mass. The final topological test also needs to be given three tracks to check the separation of the corresponding activity. This part of the selection is about identifying these three tracks.

3.1 μ Selection

A simple muon selection is employed: the longest track with a suitable particle identification (PID) score that satisfies quality requirements is chosen. The muon is occasionally broken up into several tracks (even if the activity left in the detector forms a continuous trail) due to misreconstruction, with the reconstructed vertex usually located near the start of the first one[1]. If the wrong piece is chosen this can cause problems with the connectedness test described in Section 5 and so the muon identification algorithm demands the muon candidate must start within 1 cm of the reconstructed primary vertex. The second quality requirement is that the muon candidate must be at least 10 cm in length. The PID score used is the log-likelihood ratio (LLR PID) score described in [9]. If no tracks pass these three cuts the event is rejected in its entirety.

The final part of the selection relies on comparing the positions of the activity created by the muon and the decay proton and pion and no longer works if the muon is confused with one of the decay products or another track. For this reason the PID requirement is tuned to optimise performance on signal events. Two performance metrics are calculated and presented in Figure 4. The selection uses a minimum LLR PID score of 0.6, maximising the purity while still being efficient. The efficiency and purity metrics used are:

$$\text{Efficiency} = \frac{\text{Muon candidates corresponding to true primary muons}}{\text{All muons produced at primary vertex}} \tag{2}$$

$$\text{Purity} = \frac{\text{Muon candidates corresponding to true primary muons}}{\text{All muon candidates}} \tag{3}$$

[1]It should be noted the reconstructed vertex is a distinct object from any of the tracks.

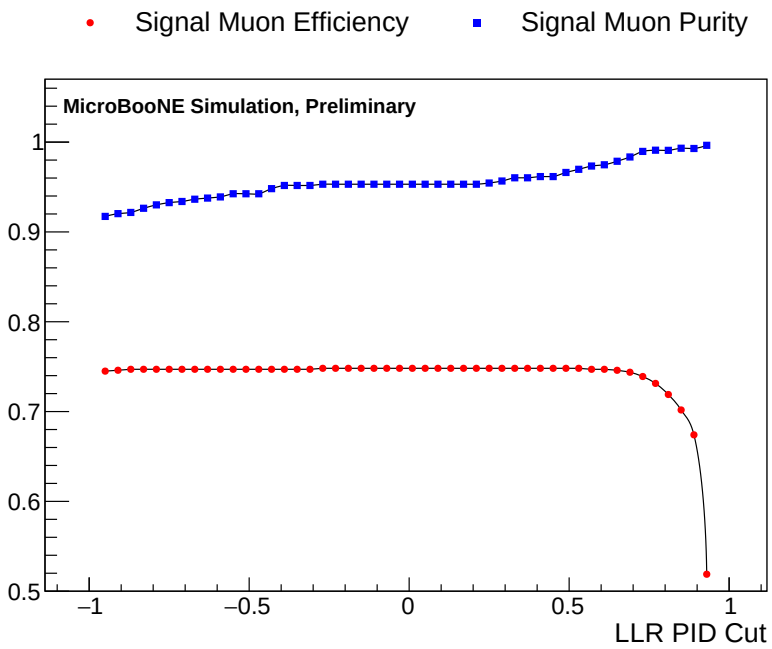

Figure 4: Performance metrics for the muon identification algorithm for different values of the minimum LLR PID score required for the muon candidate.

3.2 Decay Product Selection

If the candidate neutrino interaction has many reconstructed daughter particles there are many ways to select a pair of tracks from them as candidate decay products, and the proton and pion hypotheses may assigned in either order to a pair of tracks. There are many variables to inform this decision such as particle identification scores, the track/shower classification score produced by Pandora and geometric variables. To condense this information into a single number that is used to rank different candidates in order of preference, the Toolkit for Multivariate Analysis [10] (TMVA) from Root is employed. For each combination of tracks, several variables are calculated and analysed by an array of boosted decision trees (BDTs) to produce a response score. The following seven variables are used:

1. The separation between the starting positions of the proton/pion tracks. Both tracks should originate from a common vertex.
2. The Pandora track/shower classification score of the proton track.
3. The Pandora track/shower classification score of the pion track. This is shown to have some power to separate charged pions from other particles.
4. The mean energy deposition rate, $\langle dE/dx \rangle$, along the proton track. This is a particle identification method that separates protons from minimum ionising particles (MIPs = muons and charged pions) on very short tracks.
5. The mean energy deposition rate along the pion track.
6. The LLR PID score of the proton track, previously used in the muon identification algorithm.
7. The LLR PID score of the pion track.

These seven variables from the events used for training are presented in Figure 5. Since quantities such as the reconstructed invariant mass used by later stages of the selection will only separate the signal from background if, for the signal, the right pair of reconstructed particles are chosen, this BDT is trained to be optimal at selecting the tracks on signal only. For this reason, a pure sample of signal events in which both decay products were reconstructed is prepared and assigned a muon candidate using the algorithm described in the previous selection. Every combination of tracks and proton/pion hypotheses is formed from the remainder, those which correspond to a proton and pion from a real Λ^0 decay in the right order are the "correct" sample and all other combinations of tracks from the same events the "incorrect" sample, shown as the blue and red curves in Figure 5. The boosted decision trees are then trained to separate these two populations.

Three pre-cuts are applied to reject events containing no suitable combinations of tracks: The decay product tracks must start within 3 cm of one another, the LLR PID score of the proton candidate < 0.1 and the LLR PID score of the pion candidate > -0.1.

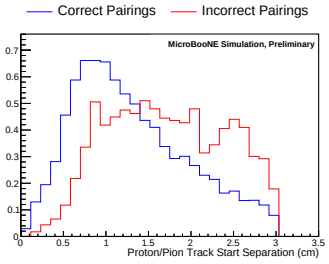

(a) Track start separation.

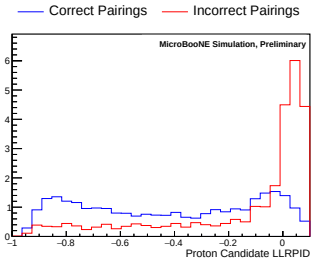

(b) Proton candidate LLR PID.

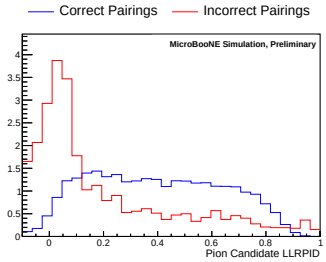

(c) Pion candidate LLR PID.

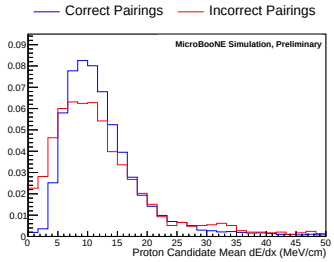

(d) Proton candidate mean dE/dx.

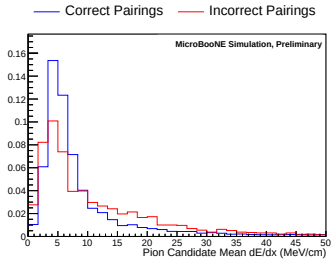

(e) Pion candidate mean dE/dx.

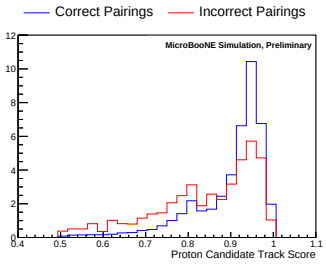

(f) Proton candidate track/shower classification score.

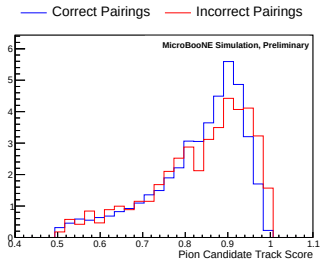

(g) Pion candidate track/shower classification score.

Figure 5: The seven variables used to select proton and pion candidates. Three pre-cuts have been applied: the track start separation < 3 cm, the proton candidate LLR PID < 0.1 and the pion candidate LLR PID > -0.1.

Figure 6 shows a breakdown of the particles chosen as the decay proton and pion candidates, indicating the correct pair of tracks are selected in around 95% of signal events. The largest components of the background are a pair of protons, a proton and pion or a pair of cosmic rays.

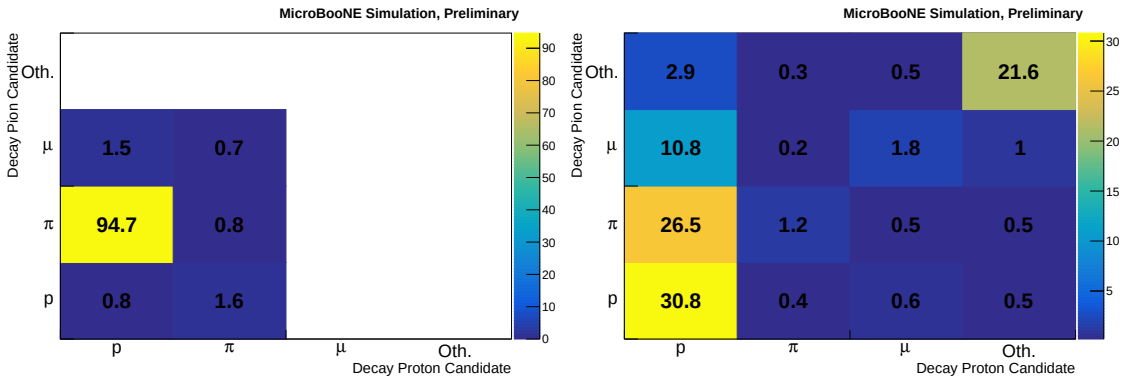

(a) Signal events.

(b) Background events.

Figure 6: Percentages of particles selected as possible decay candidates for signal and background. The "oth." (other) component is mainly comprised of cosmic rays and $e^{\pm}$.

4 Λ Decay Analysis

The distinguishing feature of Λ^0 production is the appearance of its decay products at a secondary vertex a short distance away from the primary vertex. The previous step of the selection identified a pair of tracks that might belong to a real Λ^0 decay, next the selection constructs several quantities from these two tracks to test whether these tracks are kinematically consistent with a Λ^0 decay and if they belong to a decaying particle produced at the primary vertex that has travelled a short distance.

4.1 Selection Variables

As with the identification of the decay products, to condense several variables into a single quantity that can separate signal from background, an array of boosted decision trees is employed. Three input variables are used:

1. The reconstructed invariant mass of the pair of tracks under the hypothesis they are a true proton and pion, shown in Figure 7. The Λ^0 baryon has a negligible decay width thus its decay products are always produced with a true invariant mass of 1.116 GeV/c^2. The kinematic calculations are described in Appendix A.

2. The angular deviation α: The Λ^0 should travel in a straight line from the initial neutrino interaction to the point it decays and therefore the line connecting these two positions should be parallel to the Λ^0's momentum vector. α is the angle between the reconstructed momentum vector of the Λ^0, based on the momenta of its decay products, and the line connecting the reconstructed primary vertex and the candidate decay vertex, illustrated in Figure 8. Signal and background distributions are shown in Figure 9.

3. The BDT response score from the track selector BDT described in the previous section, displayed for signal and background in Figure 10, which incorporates information about how proton/pion-like pair of tracks are.

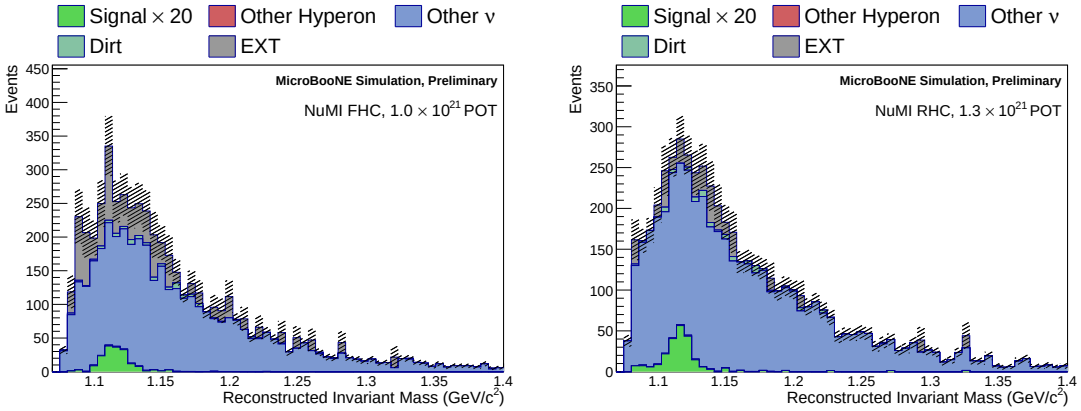

(a) GENIE FHC. (b) GENIE RHC.

Figure 7: Invariant mass of proton/pion candidates nominated by the track selector BDT. The signal component has been scaled up by a factor of 20. The hatched regions are the MC statistical uncertainties. The true mass of the Λ^0 baryon is 1.116 GeV/c^2.

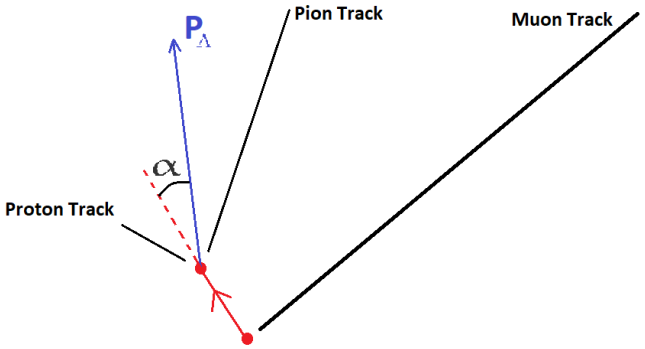

Figure 8: Definition of the angle α, the angle between the line connecting the primary and reconstructed decay vertices and the momentum vector of the combined proton and pion candidates.

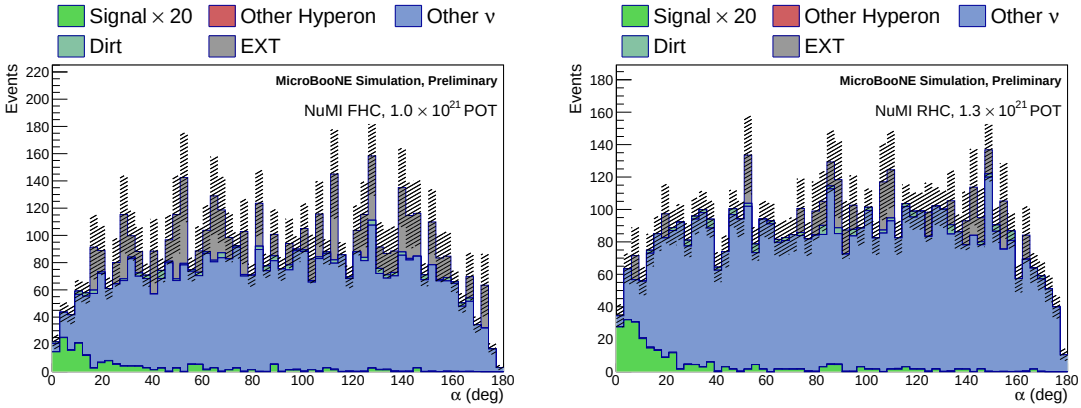

(a) GENIE FHC. (b) GENIE RHC.

Figure 9: Angular deviation α for signal and background events (illustrated in Figure 8). The signal component has been scaled up by a factor of 20.

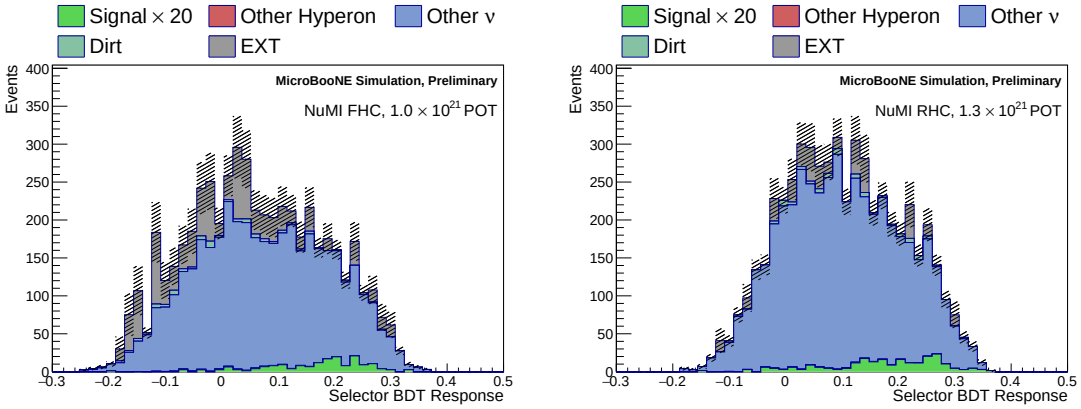

(a) GENIE FHC. (b) GENIE RHC.

Figure 10: Track selector BDT response distribution for nominated pairs of tracks. The signal component has been scaled up by a factor of 20. The hatched regions are the MC statistical uncertainties.

4.2 Performance

The variables described in Section 4.1 are used as inputs into a set of boosted decision trees and the resulting response value is calculated. The distributions for signal and background are shown in Figures 11 and 12. A large fraction of the remaining background collects at lower values of the response and thus the purity of the selection is improved by cutting events below a certain value. The selected signal and background, cutting events below various values of the response score are listed in Table 2. The significance, $S/\sqrt{S+B}$, a metric of overall performance, suggests cutting very harshly on this variable, though a significant quantity of background events remain.

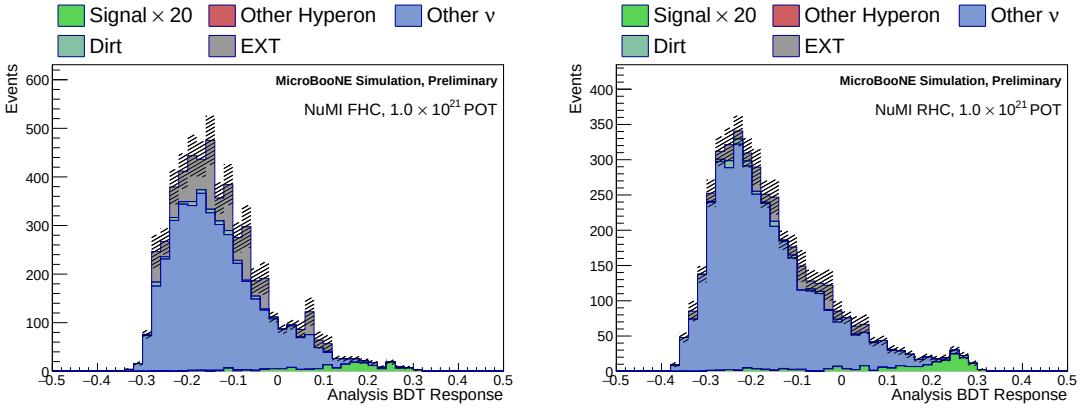

(a) GENIE FHC. (b) GENIE RHC.

Figure 11: Decay analysis BDT response distributions for the signal and background. The signal component is multiplied by 20. The hatched regions are the MC statistical uncertainties.

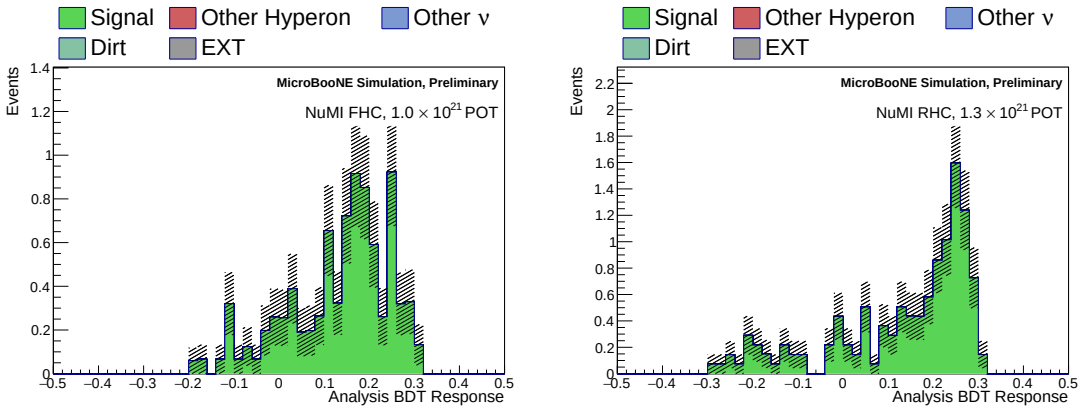

(a) GENIE FHC.

(b) GENIE RHC.

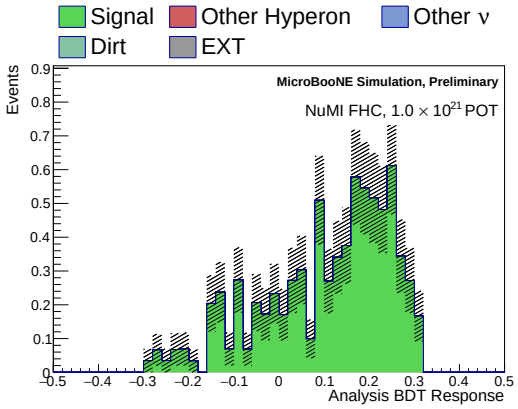

(c) NuWro FHC.

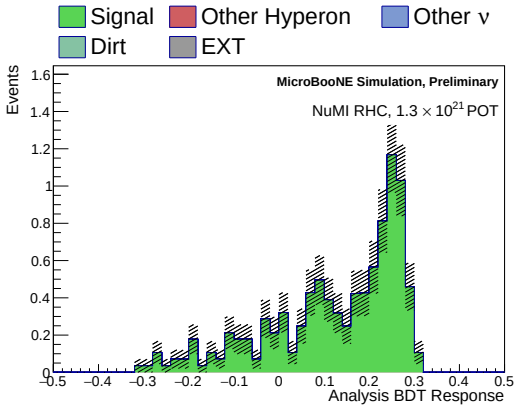

(d) NuWro RHC.

Figure 12: Decay analysis BDT response distributions for the signal, modelled with both event generators. The hatched areas indicate MC statistical uncertainties.

	FHC			RHC		
BDT Res. Cut	Sel. Signal	Sel. BG	Significance	Sel. Signal	Sel. BG	Significance
-0.2	8.5 ± 0.7	3700 ± 100	0.14	10.7 ± 0.9	2740 ± 90	0.20
-0.1	8.0 ± 0.7	1570 ± 80	0.20	9.9 ± 0.8	1260 ± 60	0.28
0.0	7.3 ± 0.7	530 ± 40	0.32	9.1 ± 0.8	490 ± 30	0.41
0.1	6.0 ± 0.6	100 ± 20	0.59	7.8 ± 0.8	130 ± 13	0.66
0.2	2.6 ± 0.4	12 ± 3	0.66	5.6 ± 0.6	20 ± 5	1.09

Table 2: Predicted event counts for different cuts of the decay analysis BDT response, using GENIE as the event generator for both signal and background. Uncertainties are MC statistical only.

5 Connectedness Tests

The feature that distinguishes a proton and pion from a Λ^0 decay from a proton and pion produced at the primary vertex with similar kinematics is that they should be produced a short distance away from the vertex due to the relatively long lifetime of the Λ^0. To make maximal use of the detector's resolution, we analyse the original filtered wire signals that the reconstructed particles are fitted to (the coloured cells shown in Figure 1). The argument is that if the proton and pion

form a separated vertex, the corresponding activity should form a separate “island" from the muon and other particles at the primary vertex.

5.1 Algorithm

The basic method is to construct a two dimensional grid, with axes being the TPC wires and time, and assign a value to each square of the grid according to how much activity was recorded on that wire at that time. This is the same information used to create the event displays in this document. A filter is then run that checks if the activity in each square is above a threshold value. Squares above this value are said to be “occupied‘. In a real $\mu + \Lambda^0$ event, the muon and decay V will form separate collections of occupied bins, while the backgrounds typically do not. This test is performed on each individual plane and if the decay is difficult to analyse in one view, for example due to undesirable orientation, it may be easier to see in the others. The same argument applies to poor quality wire activity and events affected by dead channels.

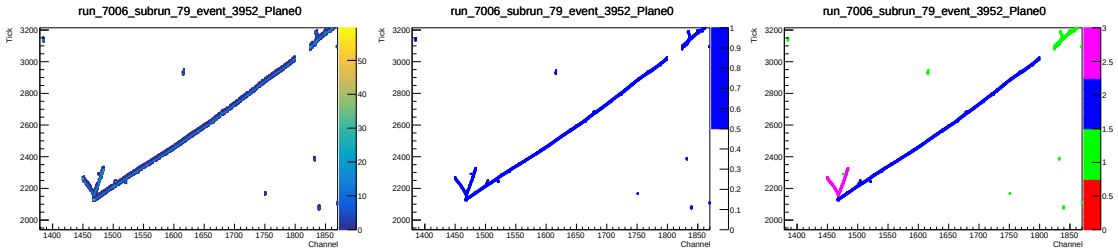

(a) Wire signals. (b) After threshold filter. (c) After clustering.

Figure 13: Three stages of generating clusters, using an event with a true muon and Λ decay, corresponding to the blue and purple clusters in (c). Green cells correspond to unused activity.

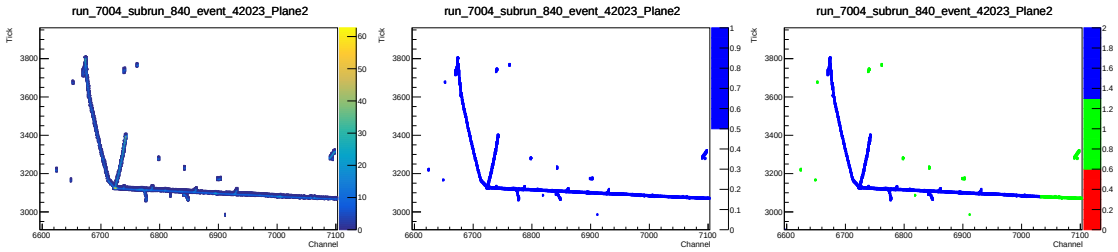

(a) Wire signals. (b) After threshold filter. (c) After clustering.

Figure 14: Three stages of generating clusters, using an event containing a background neutrino interaction. The muon (travelling to the right) overlaps and has consequently merged with the pair of secondary tracks.

To delineate the criteria for selecting events: the starting positions of the muon, decay proton and decay pion tracks are converted into wire/time space for each plane. These are used to seed the growth of clusters, and any merging that takes place is recorded. The clusters produced by the proton and pion must be recorded as merged and the muon must remain separate. Only events in which exactly this outcome occurs for at least one of the three wire planes are selected.

In addition to this, some quality cuts are applied: The clusters must both be a minimum size, span at least two channels and the seeds must not be separated by dead channels. One of the strengths of this technique is that the quality conditions can be applied to each individual plane, rejecting poor quality backgrounds whilst still being highly efficient.

6 Results

6.1 Predicted Signal and Background

The first iteration of the selection of Λ^0 production events in muon anti-neutrino interactions is complete. The step by step performance figures and predictions of the selection are displayed in Tables 3 and 4, using events generated from GENIE and NuWro respectively. The efficiencies and purities are similar for both generators despite their differing hyperon production models, an indication the selection is free of model dependence. For forward horn current, 4.1 ± 0.5 (MC stat.) signal events and 2.6 ± 1.4 background events are predicted using GENIE, giving a final efficiency of $7.6 \pm 0.9\%$ and a final purity of $60^{+20}_{-10}\%$. Using NuWro to model the signal and background neutrino interactions in the cryostat, 4.6 ± 0.5 signal events and 1.5 ± 1.4 background events are predicted, with a final efficiency of $8.2 \pm 0.9\%$ and purity of $80^{+20}_{-20}\%$. For reverse horn current simulated with GENIE, 4.9 ± 0.6 signal events and 0.5 ± 0.2 background are selected, giving an efficiency of $6.8 \pm 0.8\%$ and purity of $91^{+4}_{-5}\%$. Using NuWro to simulate reverse horn current interactions, 3.5 ± 0.5 and 0.8 ± 0.2 signal and background are selected. The resulting efficiency is $5.4 \pm 0.7\%$ and purity is $80^{+6}_{-7}\%$.

	GENIE FHC				GENIE RHC			
Cut	Signal	Background	E	P	Signal	Background	E	P
None	54 ± 2	3160000 ± 6000	1.000	0.0000	73 ± 2	3507000 ± 6000	1.000	0.0000
FV	44 ± 2	198000 ± 1000	0.805	0.0002	61 ± 2	241000 ± 1000	0.832	0.0003
Tracks	20 ± 1	34300 ± 400	0.359	0.0006	29 ± 1	45700 ± 400	0.393	0.0006
Showers	15 ± 1	20700 ± 400	0.283	0.0007	24 ± 1	26300 ± 400	0.325	0.0009
Muon ID	12.2 ± 0.9	12900 ± 300	0.223	0.0009	18 ± 1	16800 ± 300	0.245	0.0011
Decay Selector	8.5 ± 0.7	5100 ± 100	0.157	0.0016	11.4 ± 0.9	5100 ± 100	0.156	0.0022
Decay Analysis	4.7 ± 0.6	29 ± 5	0.086	0.1406	5.6 ± 0.6	20 ± 5	0.077	0.2145
Connectedness	4.1 ± 0.5	2.6 ± 1.4	0.076	0.6125	4.9 ± 0.6	0.5 ± 0.2	0.068	0.9066

Table 3: Accepted signal and background and corresponding performance metrics at each stage of the selection, using GENIE events. Uncertainties are MC statistical only. The fiducial volume (FV), track and shower cuts described in section 2 are first applied, a muon candidate using the algorithm in section 3.1 is identified. The decay proton and pion tracks are selected as explained in section 3.2 and several quantities associated with the decay are analysed to reject much of the background in section 4. Finally the connectedness test from section 5 is performed.

	NuWro FHC				NuWro RHC			
Cut	Signal	Background	E	P	Signal	Background	E	P
None	56 ± 2	3194000 ± 6000	1.000	0.0000	64 ± 2	3558000 ± 6000	1.000	0.0000
FV	45 ± 2	209000 ± 1000	0.802	0.0002	55 ± 2	255000 ± 1000	0.842	0.0002
Tracks	20 ± 1	34100 ± 400	0.357	0.0006	25 ± 1	45600 ± 500	0.387	0.0006
Showers	17 ± 1	21400 ± 400	0.298	0.0008	20 ± 1	27600 ± 400	0.306	0.0007
Muon ID	13.1 ± 0.9	13900 ± 300	0.235	0.0009	16 ± 1	17900 ± 300	0.245	0.0009
Decay Selector	9.0 ± 0.7	5300 ± 100	0.161	0.0017	10.3 ± 0.8	5200 ± 100	0.158	0.0020
Decay Analysis	5.3 ± 0.6	36 ± 7	0.097	0.130	4.3 ± 0.5	12 ± 4	0.066	0.2567
Connectedness	4.6 ± 0.5	1.5 ± 1.4	0.082	0.7515	3.5 ± 0.5	0.8 ± 0.2	0.054	0.8111

Table 4: Accepted signal and background and corresponding performance metrics at each stage of the selection, using NuWro events. Uncertainties are MC statistical only.

6.2 Phase Space

The efficiency of the entire selection as a function of the Λ^0's momentum is calculated to check for non-uniformity and presented in Figure 15. If the Λ^0 is of very low or very high momenta it becomes difficult to reconstruct, either because the decay products do not travel far enough to leave a clear signature or are too co-linear to separate into two tracks. A partial phase space cross section measurement, excluding these regions, should be considered for the final analysis. The efficiency curves are similar for both NuWro and GENIE hyperon samples, indicating the selection efficiency does not have any strong dependence on the underlying hyperon production model.

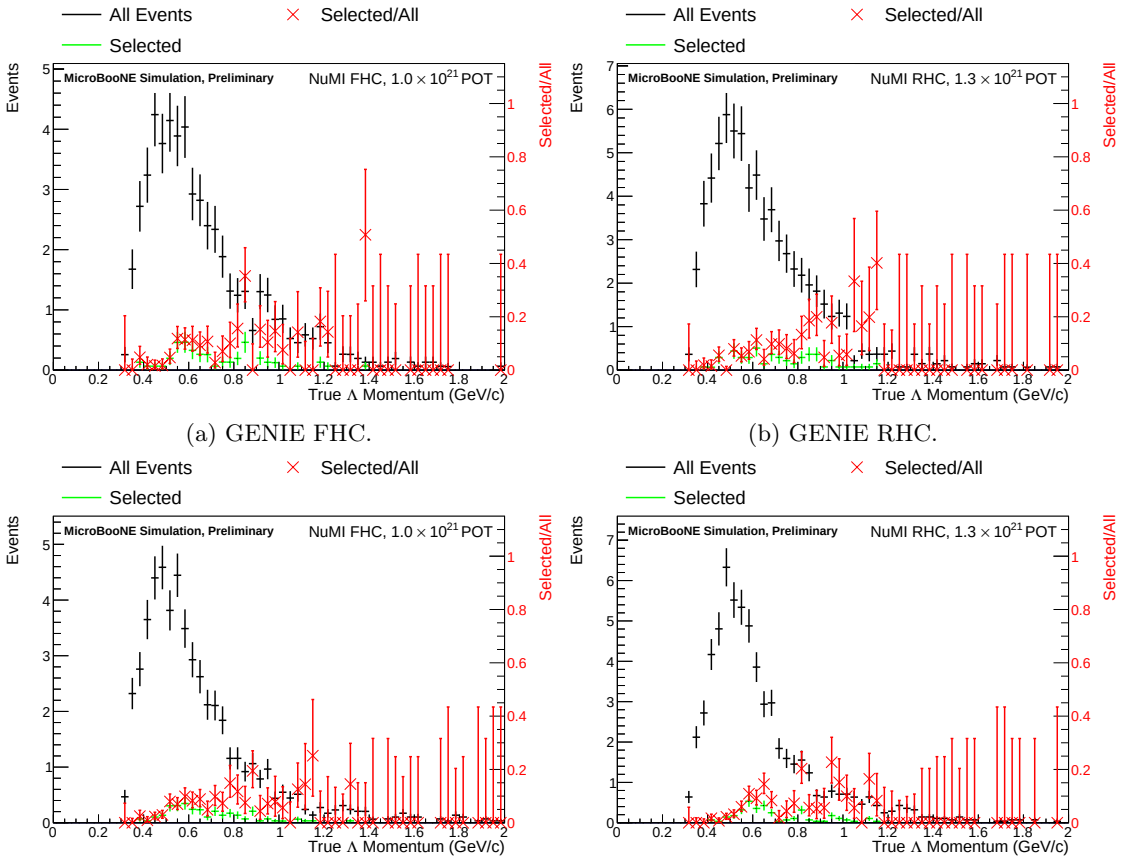

(a) GENIE FHC.

(b) GENIE RHC.

(c) NuWro FHC.

(d) NuWro RHC.

Figure 15: Efficiency of the complete selection as a function of the Λ true momentum. The uncertainties are calculated with the TEfficiency class [11] from Root using a Bayesian method with a uniform prior.

6.3 Selected Background Types

The remaining backgrounds may be split into three categories:

1. Events in which there is a small gap in the activity left by the muon close to the vertex. Removing these is the reason the muon identification algorithm requires the muon track starts within 1 cm of the reconstructed primary vertex. A possible method to reject this source of background is hand scanning the selected events.

2. Events with an energetic neutron in the final state that underwent a secondary interaction producing a pair of charged particles (typically a pair of protons or a proton and charged

pion) with similar kinematics to a Λ^0 decay. An example is shown in Figure 16. While topologically this is similar, these events are distinguished by their kinematics and PID values in the case of $p + p$ production. The removal of much of this background is a benefit of using this additional information as can be seen by the steady reduction in the quantity of background as the minimum analysis BDT response value is increased.

3. Other sources of Λ^0 baryons; a mixture of direct Λ^0 events not classified as signal because their decay products did not satisfy our kinematic requirements and events containing a Σ^0 in the final state (which subsequently decays via $\Sigma^0 \to \Lambda^0 + \gamma$).

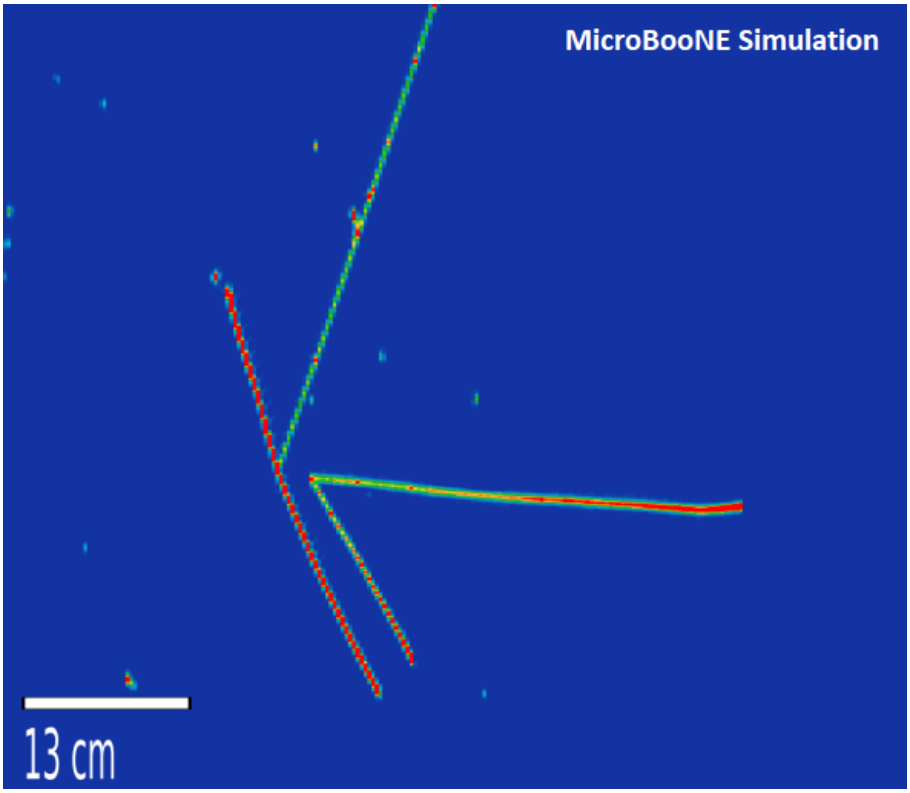

Figure 16: An event containing a neutron scatter that resulted in a proton and pion forming the V shape. Thus was mistaken for a Λ decay and selected.

6.4 Outlook

Given the statistically limited nature of this analysis, the final goal is to perform flux averaged total cross section measurements for each flux and/or both fluxes combined. To complete the cross section measurement, the generator, reinteraction and detector systematics must be evaluated.

The dominant remaining background is the result of neutron scatters though the MC statistics are severely limited. A proposed solution is to generate dedicated samples containing neutron scatters. Reinteraction systematics may be evaluated with Geant 4 Reweight [12] which is used to propagate hadron reinteraction uncertainties through reweighting, though this package does not currently include hyperons.

References

[1] Christopher Thorpe et al. "Second class currents, axial mass, and nuclear effects in hyperon production". In: *Phys. Rev. C* 104.3 (2021), p. 035502. DOI: 10.1103/PhysRevC.104.035502. arXiv: 2010.12361 [hep-ph].

[2] C. Andreopoulos et al. "The GENIE Neutrino Monte Carlo Generator". In: *Nucl. Instrum. Meth. A* 614 (2010), pp. 87–104. arXiv: 0905.2517 [hep-ph].

[3] T. Golan, J. T. Sobczyk, and J. Zmuda. "NuWro: the Wroclaw Monte Carlo Generator of Neutrino Interactions". In: *Nucl. Phys. B Proc. Suppl.* 229-232 (2012). Ed. by George S. Tzanakos, pp. 499–499.

[4] S. Agostinelli et al. "GEANT4–a simulation toolkit". In: *Nucl. Instrum. Meth. A* 506 (2003), pp. 250–303. DOI: 10.1016/S0168-9002(03)01368-8.

[5] J. S. Marshall et al. "The Pandora multi-algorithm approach to automated pattern recognition in LAr TPC detectors". In: *J. Phys. Conf. Ser.* 888.1 (2017), p. 012142.

[6] P. A. Zyla et al. "Review of Particle Physics". In: *PTEP* 2020.8 (2020), p. 083C01.

[7] P. Abratenko et al. "Cosmic Ray Background Rejection with Wire-Cell LArTPC Event Reconstruction in the MicroBooNE Detector". In: (Jan. 2021). arXiv: 2101.05076 [physics.ins-det].

[8] P. Abratenko et al. "Measurement of space charge effects in the MicroBooNE LArTPC using cosmic muons". In: *JINST* 15.12 (2020), P12037. DOI: 10.1088/1748-0221/15/12/P12037. arXiv: 2008.09765 [physics.ins-det].

[9] P. Abratenko et al. "Calorimetric classification of track-like signatures in liquid argon TPCs using MicroBooNE data". In: (Aug. 2021). arXiv: 2109.02460 [physics.ins-det].

[10] Andreas Hocker et al. "TMVA - Toolkit for Multivariate Data Analysis". In: (Mar. 2007). arXiv: physics/0703039.

[11] https://root.cern.ch/doc/master/classTEfficiency.html. Accessed August 2021. Root version 6.16 used.

[12] J. Calcutt et al. "Geant4Reweight: a framework for evaluating and propagating hadronic interaction uncertainties in Geant4". In: *JINST* 16.08 (2021), P08042. DOI: 10.1088/1748-0221/16/08/P08042. arXiv: 2105.01744 [physics.data-an].

[13] https://nusoft.fnal.gov/larsoft/doxsvn/html/classtrkf_1_1TrackMomentumCalculator.html. Accessed July 2021. LArSoft version 08.05.00.13 was used.

Appendices

A Kinematics

The momenta of the proton and pion candidates are calculated from the lengths and directions of their respective tracks [13]:

$$E_k = 29.93R^{0.5863} \qquad \mathbf{p}_{\text{proton}} = \sqrt{E_k^2 + 2M_p E_k}\hat{\mathbf{n}}_{\text{p}} \tag{4}$$

$$\mathbf{p}_\pi = \left(14.96 + 0.004349R - 14.688R^{-0.1169}\right)\hat{\mathbf{n}}_\pi \tag{5}$$

Where R is the length of the track and $\hat{\mathbf{n}}$ the direction at the start of the track.

B Efficiencies

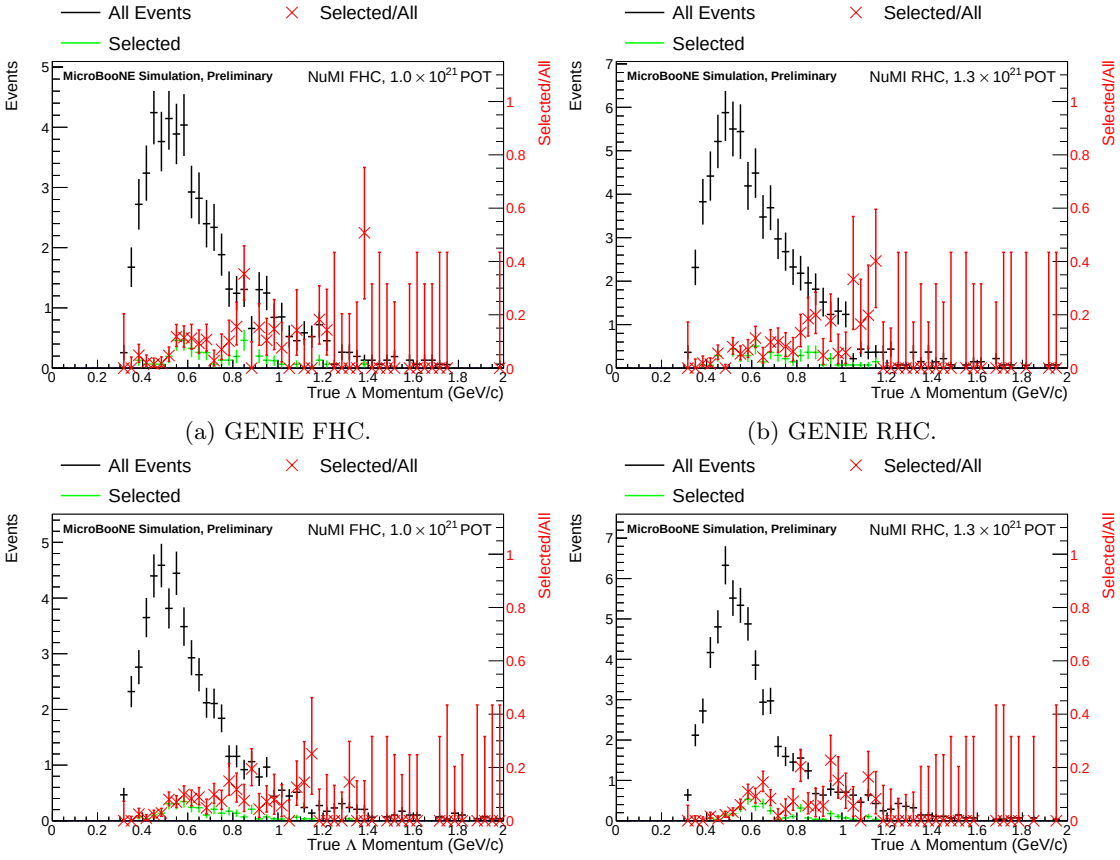

(a) GENIE FHC.

(b) GENIE RHC.

(c) NuWro FHC.

(d) NuWro RHC.

Figure 17: Efficiency of the complete selection as a function of the Λ true momentum. The uncertainties are calculated with the TEfficiency class [11] from Root using a Bayesian method with a uniform prior.

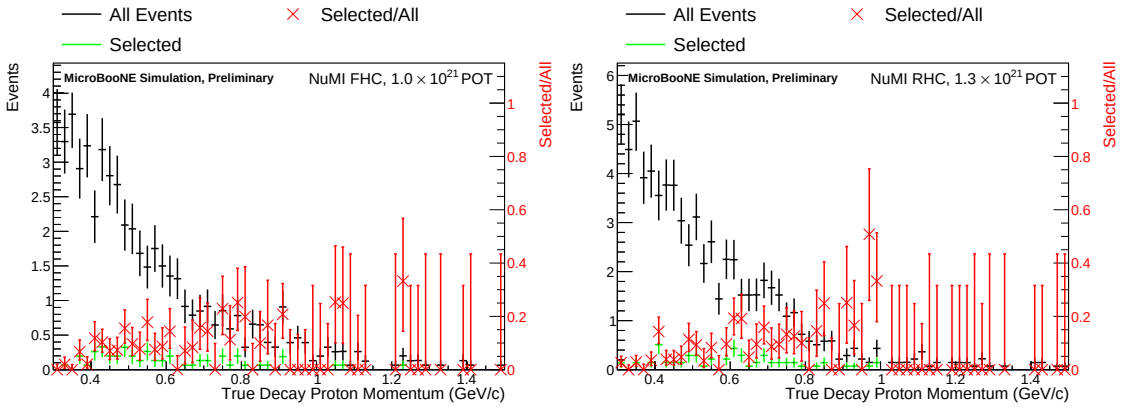

(a) GENIE FHC.

(b) GENIE RHC.

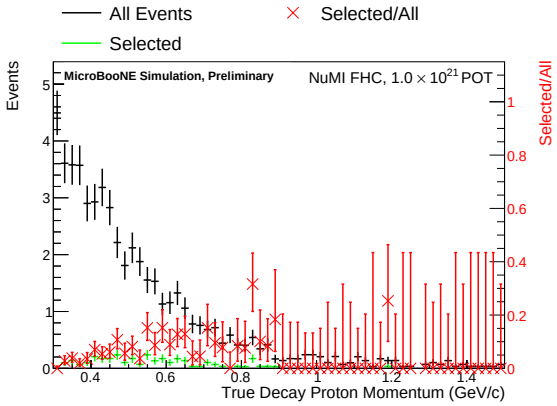

(c) NuWro FHC.

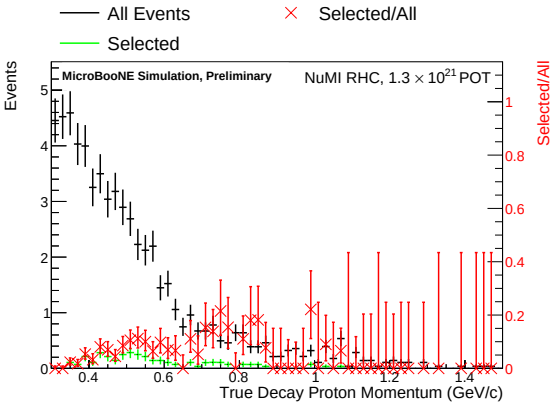

(d) NuWro RHC.

Figure 18: Efficiency of the complete selection as a function of the decay proton's true momentum. The uncertainties are calculated with the TEfficiency class [11] from Root using a Bayesian method with a uniform prior.

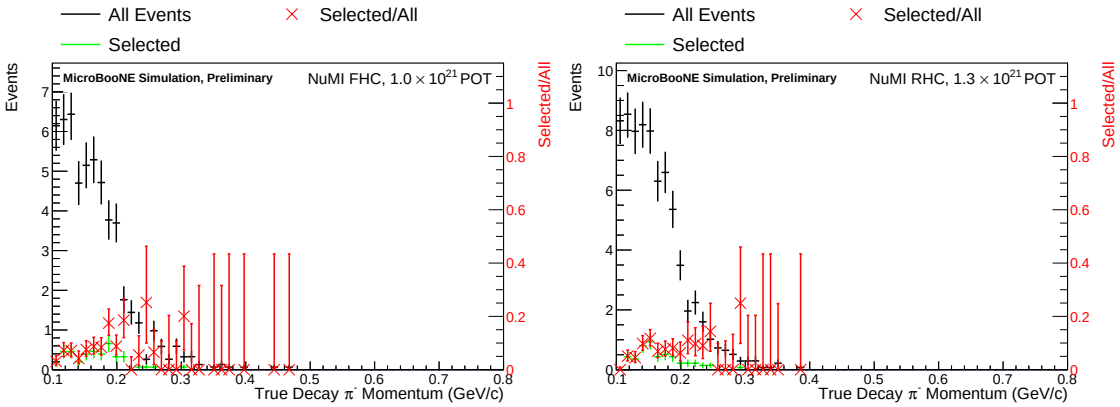

(a) GENIE FHC.

(b) GENIE RHC.

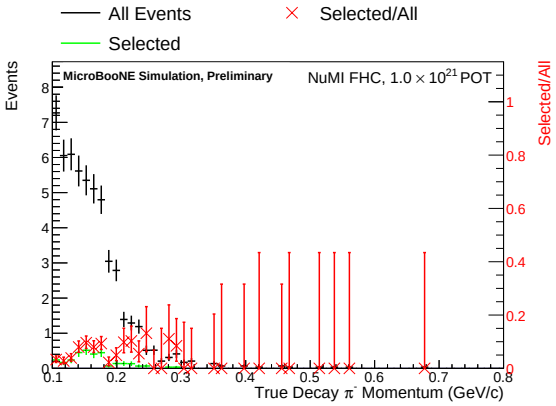

(c) NuWro FHC.

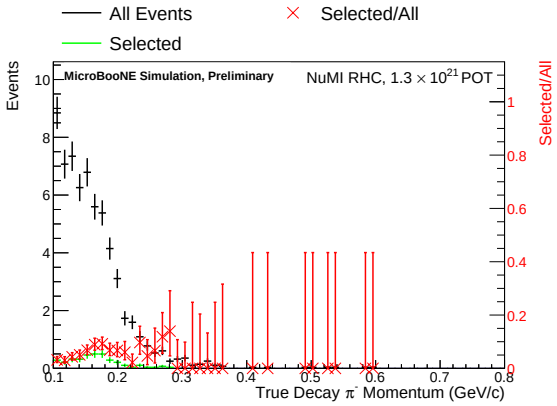

(d) NuWro RHC.

Figure 19: Efficiency of the complete selection as a function of the decay π^-'s true momentum. The uncertainties are calculated with the TEfficiency class [11] from Root using a Bayesian method with a uniform prior.

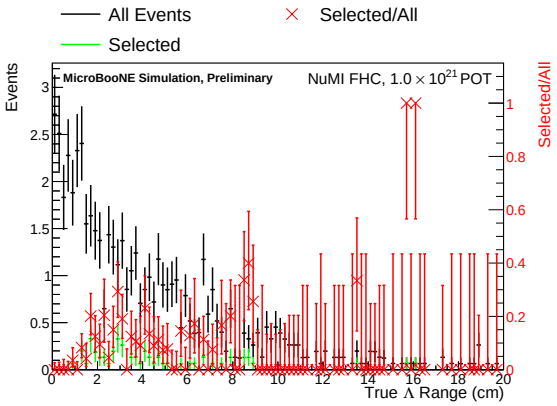

(a) GENIE FHC.

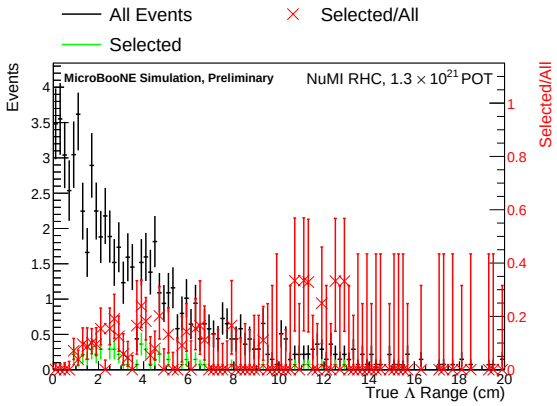

(b) GENIE RHC.

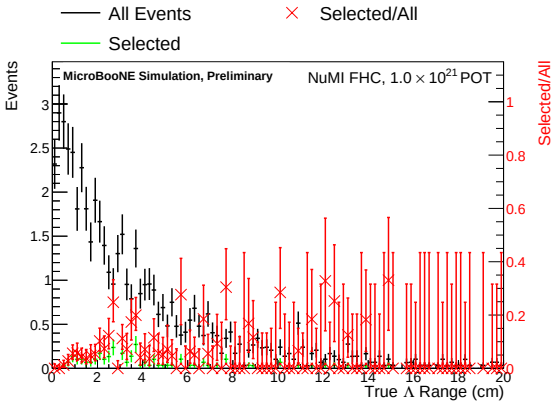

(c) NuWro FHC.

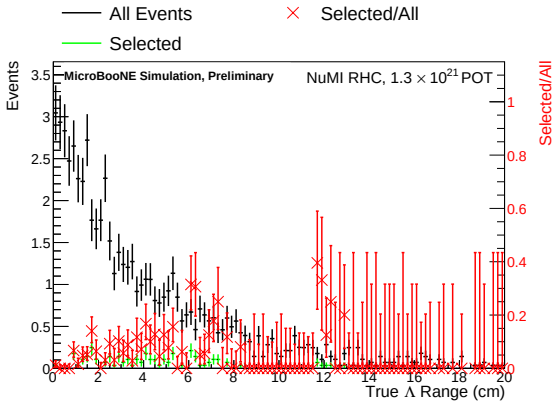

(d) NuWro RHC.

Figure 20: Efficiency of the complete selection as a function of the Λ's true range. The uncertainties are calculated with the TEfficiency class [11] from Root using a Bayesian method with a uniform prior.

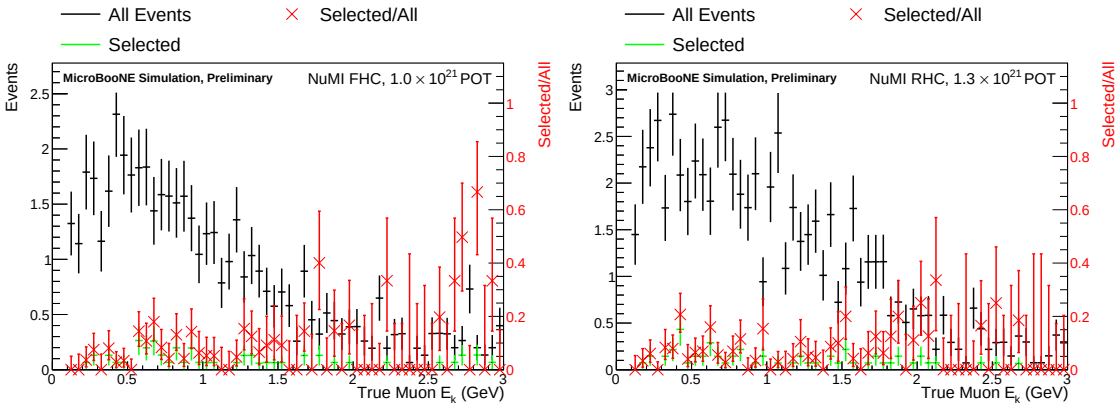

(a) GENIE FHC.

(b) GENIE RHC.

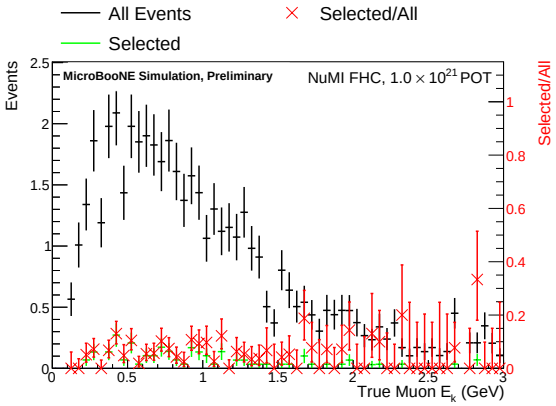

(c) NuWro FHC.

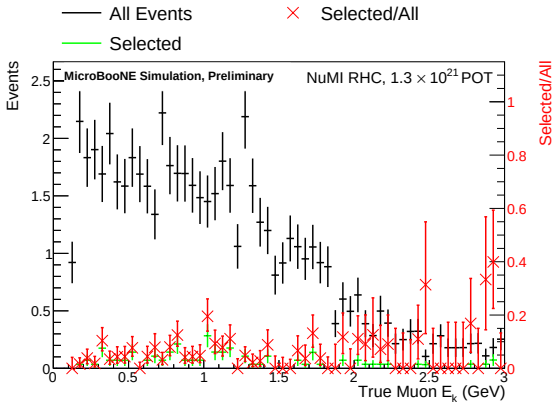

(d) NuWro RHC.

Figure 21: Efficiency of the complete selection as a function of the μ^+'s kinetic energy. The uncertainties are calculated with the TEfficiency class [11] from Root using a Bayesian method with a uniform prior.

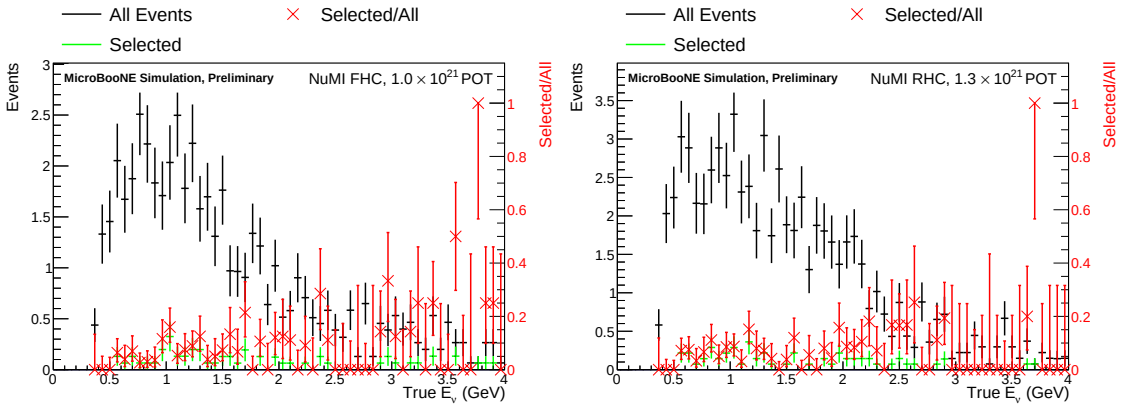

(a) GENIE FHC.

(b) GENIE RHC.

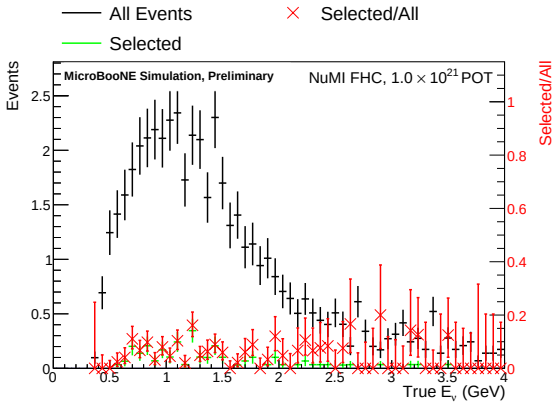

(c) NuWro FHC.

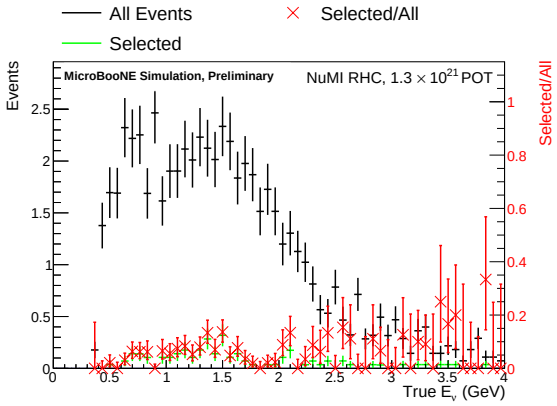

(d) NuWro RHC.

Figure 22: Efficiency of the complete selection as a function of the true anti-neutrino energy. The uncertainties are calculated with the TEfficiency class [11] from Root using a Bayesian method with a uniform prior.

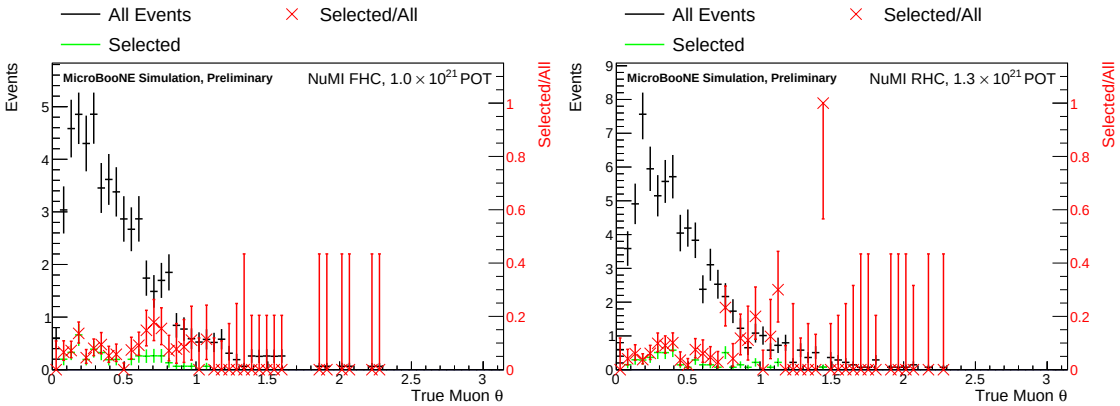

(a) GENIE FHC.

(b) GENIE RHC.

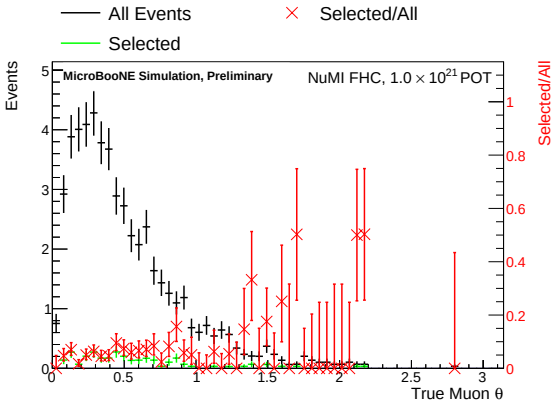

(c) NuWro FHC.

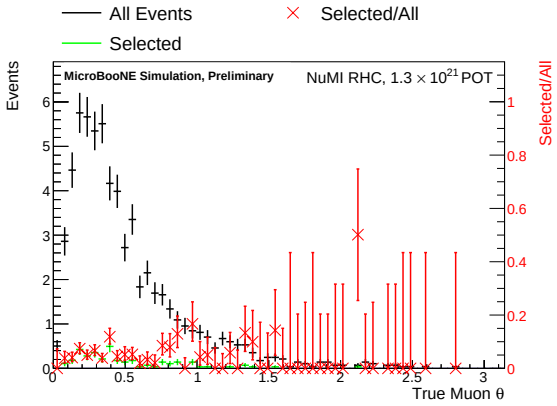

(d) NuWro RHC.

Figure 23: Efficiency of the complete selection as a function of the true scattering angle of the μ^+. The uncertainties are calculated with the TEfficiency class [11] from Root using a Bayesian method with a uniform prior.